Journal of Sound and Vibration (1996) **194**(3), 417–437

HIGH FREQUENCY RESPONSE OF A FLUID-FILLED CYLINDRICAL SHELL WITH AN INTERNAL COLUMN OF GAS BUBBLES: APPLICATION TO ACTIVE ACOUSTIC GAS LEAK DETECTION

B. J. BRÉVART† AND C. JOURNEAU

Commissariat à l'Energie Atomique, Laboratoire de Systèmes de Mesure et d'Instrumentation, Centre de Cadarache, 13108 *St Paul lès Durance Cedex, France*

AND

C. R. FULLER

Vibration and Acoustics Laboratories, Mechanical Engineering Department, Virginia Polytechnic Institute and State University, Blacksburg, VA 24061-0238, *U.S.A.*

(*Received* 13 *October* 1994, *and in final form* 4 *December* 1995)

The high frequency response to a point force excitation of an infinite elastic cylindrical shell, filled with a liquid including a column of gas bubbles, is investigated. A state vector approach is used for the shell theory to include the effects of shear deformation and rotary inertia. The far field mobility of the shell for each propagating circumferential mode n is calculated using a residue method. Each of these residues are evaluated at the poles k_{ns} of the infinite coupled system. The waves associated with axial wavenumbers of the same type (order s) reveal similar characteristics in the fluid field, such as the number of radial nodal lines, and the corresponding residues are thus grouped together. The resulting wave type decomposition of the system response carries important information. At the non-dimensional $\Omega = 10$ for the shell studied, the response of the system is dominated by $s = 1$ waves and a column of gas bubbles in the fluid field is difficult to detect by its effects on the vibrations of the shell. As the frequency is increased (to $\Omega = 50$, for example), the system response is dominated by waves of increasing type order ($s = 15, 16, \ldots,$) and a column of gas bubbles has the effect of bringing a large attenuation to the shell response. Various experiments were performed to verify these results.

1. INTRODUCTION

In order to optimize the performances of an active ultrasonic gas bubble detector developed by the CEA [1], a good understanding of the wave propagation mechanisms in fluid-filled cylindrical elastic shells at high frequencies ($\Omega \geqslant 10$) is required.

The low non-dimensional frequency region ($\Omega \leqslant 3$) has been extensively studied by several authors. Fuller and Fahy first characterized the system behavior in terms of propagation and power flow of free waves [2]. They gave physical interpretations of the

†B. J. Brévart is currently working at Alcatel Alsthom Recherche, Marcoussis, France. This work was performed at VPI & SU as a co-operative arrangement between the CEA and the VAL of VPI & SU during his military service (CSN/STS).

0022–460X/96/280417 + 21 $18.00/0

eigen values and determined the energy distributions (or power) within the coupled system. Fuller then considered the problem of structural excitation by a radial line force and internal monopole excitation [3, 4]. More recently, Leyrat investigated the characteristics of wave propagation in fluid-filled shells including a uniform internal flow and presented a solution for the mobility of both infinite and finite systems [5]. Brévart and Fuller then extended the previous investigations by evaluating the effect of the flow on the distribution of vibrational energy in the system [6]. Feng performed experimental studies of the structural response and the acoustic radiation of infinite and finite fluid-filled shells [7]. He recently explained some unexpected experimental results by adding to the model of a fluid-filled shell the effect of an absorptive layer on the inner side of the wall [8]. All of these investigations were based on simplified shell equations such as the Donnell–Mushtari or the Kennard equations. They do not include the effects of transverse shear forces or rotary inertia and are only valid at relatively low frequencies.

To include to the shell model shear deformation and rotary inertia effects, Borgiotti and Rosen [9] used the full elasticity theory applied to thin shells and a state vector formalism. Using this technique, they initially investigated the power flow analysis of the forced vibrations of infinite cylinders in vacuum [9]. Recently, they extended this power flow analysis to surface waves on cylindrical elastic shells immersed in an acoustic fluid, focusing principally on the low frequency regime [10].

To date, literature concerning vibrations of liquid-filled cylinders at very high frequencies is scarce. Journeau recently considered the problem [11]. He developed a simplified modal approach based on the Timoshenko–Mindlin plate equation, i.e., including transverse shear deformations and rotary inertia but neglecting the shell curvature. Using this model, he determined scaling laws between a liquid filled cylinder and another cylinder filled with a different liquid.

In this paper, the state vector technique developed for the shell model by Borgiotti and Rosen [9] is utilized to study the high frequency response of infinite elastic cylinders filled with a fluid incorporating a column of gas bubbles. The dispersion of the propagating waves in the system at high frequencies is first considered and analyzed. The mobility of the system excited by a point force is then computed using a residue theorem. This technique allows one to determine the individual contribution of each wave in the system. It is found that the nature of the dominating waves in the system varies drastically with frequency, and that this explains the variations in the performances of a gas leak monitoring system based on the shell response. The major point raised by the analytical investigation are experimentally verified.

2. THEORY: THE STATE VECTOR APPROACH

The theory that follows is based on the state vector formalism developed by Borgiotti and Rosen for "thick" cylindrical shells [9, 10]. By "thick" shells is meant shells, the thickness of which exceeds a twentieth of the shear wavelength, as in Timoshenko's theory on beams. The model was established from the 3-D stress–strain relationships, reduced to 2-D by integration through the shell thickness. It was assumed that the radial normal stress is negligible and that the velocity vector varies linearly with the radial co-ordinate. These assumptions are valid for a shell with a small thickness to radius ratio, as in the case considered here ($h/a = 0{\cdot}03$).

For brevity, only the most important steps of the derivation are recalled in this paper, and the reader should thus refer to references [9, 10] for more details. A list of symbols is included in Appendix B.

2.1. CHARACTERISTIC EQUATION

If $p(z, n)$ is the pressure created by the fluid loading at the wall, the motion of the cylindrical shell can be described by a tenth order system of differential equations [9, 10],

$$\frac{d\mathbf{x}(z, n)}{dz} - \mathbf{M}(n)\mathbf{x}(z, n) = p(z, n)\mathbf{c}. \tag{1}$$

where $\mathbf{M}(n)$ is a 10×10 matrix, the elements of which are defined in Appendix A. The transpose of the column vector $\mathbf{c}$ is

$$\mathbf{c}^T = (-1, 0, 0, 0, 0, 0, 0, 0, 0, 0). \tag{2}$$

The transpose of the state vector $\mathbf{x}(z, n)$ is

$$\mathbf{x}^T(z, n) = (T_{z\rho}, T_{z\varphi}, N_z, M_z, M_{z\varphi}, v_\rho, v_\varphi, v_z, \Omega_z, \Omega_\varphi). \tag{3}$$

Considering the shell element in Figure 1, $T_{z\rho}$ and $T_{z\varphi}$ are, respectively, the ρ and φ components of the shear force resultant per unit circumferential length on the face $z =$ constant. N_z is the normal force resultant per unit circumferential length. M_z and $M_{z\varphi}$ are, respectively, the bending and twisting moment resultants in the ρ–z and ρ–φ planes per unit circumferential length on the face $z =$ constant. v_ρ, v_φ and v_φ are the velocity components of a mid-fiber point. Ω_z and Ω_φ are the angular velocities in the ρ–z and ρ–φ planes.

Solutions of equation (1) associated with an axial wavenumber k_{ns} can be expressed as

$$\mathbf{x}(z, n) = \mathbf{e}^s(n)\, e^{-jk_{ns}z}, \tag{4}$$

where $\mathbf{e}^s(n)$ is a column vector independent of z.

Let $Z(k_{ns}, n)$ be the acoustic impedance of the fluid at the shell wall. Then, the pressure can be written as

$$p(z, n) = Z(k_{ns}, n)v_p^s(n)\, e^{-jk_{ns}z}. \tag{5}$$

Introducing the expressions (4) and (5) into equation (1), one obtains

$$[-jk_{ns}\mathbf{I} - \mathbf{M}(n)]\, \mathbf{e}^s(n) - Z(k_{ns}, n)\mathbf{c}v_p^s(n) = 0. \tag{6}$$

Since $v_p^s(n)$ is the sixth term of $\mathbf{e}^s(n)$, equation (6) can be rewritten as

$$[-jk_{ns}\mathbf{I} - \mathbf{M}^{[1]}(n)]\, \mathbf{e}^s(n) = 0, \tag{7}$$

where $\mathbf{M}^{[1]}$ is a matrix defined as

$$M_{ij}^{[1]} = M_{ij}, \quad \text{if } i \neq 1, j \neq 6, \qquad M_{16}^{[1]} = M_{16} - Z(k_{ns}, n). \tag{8}$$

For equation (7) to have a non-trivial solution, we must have

$$|-jk_{ns}\mathbf{I} - \mathbf{M}^{[1]}(n)| = 0, \tag{9}$$

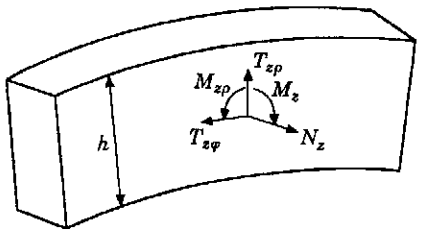

Figure 1. The shell element ($z =$ constant).

where | | denotes the determinant of the matrix. Equation (9) is the characteristic equation of the system, the roots of which are found numerically. In this analysis, we are only concerned with the propagating waves in the system; i.e., the real roots of equation (9). These roots will become complex, with a relatively small imaginary part, if damping is added to the system, in the shell wall or the fluid field. The reader is referred to section 2.4.1 for details of the root-finding approach.

2.2. ACOUSTIC IMPEDANCE AT THE SHELL WALL

To account for the presence of gas bubbles in the fluid, the acoustic field is divided in two coaxial media A and B with different properties, as indicated in Figure 2.

The acoustic properties of water containing gas bubbles depend on the volume ratio of air to water, on the bubble size and on the imposed frequency [12]. The effects of the bubbles on the water properties are of two kinds: first, the speed of sound is altered and, then, the sound waves are damped [12].

It is first assumed that the percentage of gas in medium B is small enough not to decrease the density of the fluid. In addition, it is assumed that the bubble size is much smaller than the acoustic wavelength in the fluid and that the frequencies considered in this analysis are well above the resonant frequencies of the bubbles. Note that these two assumptions actually define an extremely large range of bubble sizes, varying from one millimeter to one centimeter in diameter around 50 kHz, for example.

If the three conditions above are respected, the alteration of the speed of sound due to the presence of gas bubbles is negligible and the bubbles only cause the sound waves to be damped [12].

Let c_f^d be the free wave speed in medium B and let β be the attenuation constant of the fluid due to the gas bubbles. Then

$$c_f^d = c_f(1 + \beta \mathrm{j}), \tag{10}$$

where c_f is the free wave speed of the lossless fluid A.

Let p^d and p^f be the acoustic pressures in media B and A, respectively. They can be expressed as

$$p^d(z, r, \varphi) = \sum_{n=0}^{\infty} \sum_{s=1}^{\infty} [P_{ns}^d \mathrm{J}_n(k_{rns}^d r)] \cos(n\varphi)\, \mathrm{e}^{-\mathrm{j}k_{ns}^d z}, \tag{11}$$

$$p^f(z, r, \varphi) = \sum_{n=0}^{\infty} \sum_{s=1}^{\infty} [P_{ns}^f \mathrm{J}_n(k_{rns}^f r) + Q_{ns}^f \mathrm{Y}_n(k_{rns}^f r)] \cos(n\varphi)\, \mathrm{e}^{-\mathrm{j}k_{ns}^f z}, \tag{12}$$

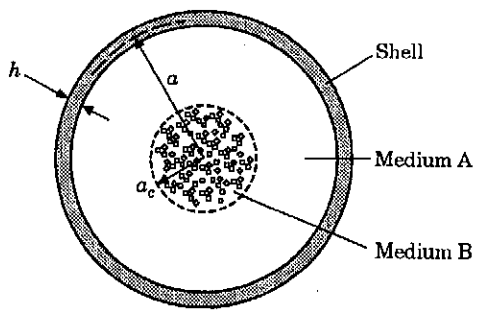

Figure 2. The cylinder cross-section.

where k^d_{rns} and k^f_{rns} are the radial wavenumbers in the two fluid media, defined as

$$k^d_{rns} = \pm\sqrt{(\omega/c^d_f)^2 - k^2_{ns}}, \qquad k^f_{rns} = \pm\sqrt{(\omega/c_f)^2 - k^2_{ns}}. \tag{13, 14}$$

Applying the boundary conditions, continuity of the particle velocity at the shell–fluid interface and continuity of the acoustic pressure and velocity at the fluid A–fluid B interface, one eventually obtains [8] the pressure amplitudes in equation (12).

$$P^f_{ns} = v^s_p(n)D_1/\Delta, \qquad Q^f_{ns} = v^s_p(n)D_2/\Delta, \tag{15, 16}$$

where

$$\begin{aligned}\Delta = {} & \rho_f k^d_{rns} \mathrm{J}'_n(x^d_B)[\mathrm{J}_n(x^f_B)\mathrm{Y}'_n(x^f_A) - \mathrm{J}'_n(x^f_A)\mathrm{Y}_n(x^f_B)] \\ & + \rho_d k^f_{rns} \mathrm{J}_n(x^d_B)[\mathrm{J}'_n(x^f_A)\mathrm{Y}'_n(x^f_B) - \mathrm{J}'_n(x^f_B)\mathrm{Y}'_n(x^f_A)]\end{aligned} \tag{17}$$

$$D_1 = -\mathrm{j}\omega\left[\rho_f\rho^d_f \mathrm{J}_n(x^d_A)\mathrm{Y}'_n(x^f_A) - \frac{\rho^2_f k^d_{rns}}{k^f_{rns}} \mathrm{J}'_n(x^d_B)\mathrm{Y}_n(x^f_B)\right], \tag{18}$$

$$D_2 = -\mathrm{j}\omega\left[\rho_f\rho^d_f \mathrm{J}_n(x^d_A)\mathrm{J}'_n(x^f_A) + \frac{\rho^2_f k^d_{rns}}{k^f_{rns}} \mathrm{J}'_n(x^d_B)\mathrm{J}_n(x^f_B)\right], \tag{19}$$

ρ_f and ρ^d_f are the specific masses of the fluid media. The arguments of the Bessel functions are defined as

$$x^f_A = k^f_{rns}(a - h/2), \qquad x^d_A = k^d_{rns}(a - h/2), \qquad x^f_B = k^f_{rns}a_c, \qquad x^d_B = k^d_{rns}a_c, \tag{20}$$

where a_c is the radius of the medium B column, a is the mean radius of the shell and h is the thickness of the shell.

The acoustic impedance at the shell wall is then given by

$$Z(k_{ns}, n) = [D_1\mathrm{J}_n(x^f_A) + D_2\mathrm{Y}_n(x^f_A)]/\Delta. \tag{21}$$

2.3. FORCED RESPONSE OF THE COUPLED SYSTEM

To find the response of the complete system to a radial line force $F_p\delta(z)\cos(n\varphi)$, the state vector $\mathbf{x}(z, n)$ is first defined by its integral in the wavenumber domain,

$$\mathbf{x}(z, n) = \frac{1}{2\pi}\int_{-\infty}^{+\infty} \hat{\mathbf{x}}(k, n)\,\mathrm{e}^{-\mathrm{j}k_n z}\,\mathrm{d}k_n. \tag{22}$$

Including the internal acoustic field and the input force on the shell wall, the equation of motion (1) is expressed as

$$\frac{\mathrm{d}\mathbf{x}(z, n)}{\mathrm{d}z} - \mathbf{M}^{\mathrm{fl}}(n)\mathbf{x}(z, n) = \mathbf{q}\delta(z), \tag{23}$$

where

$$\mathbf{q}^{\mathrm{T}} = \frac{1}{2\pi a}(F_p, 0, 0, 0, 0, 0, 0, 0, 0, 0). \tag{24}$$

In the wavenumber domain, equation (23) becomes

$$[-\mathrm{j}k_n\mathbf{I} - \mathbf{M}^{\mathrm{fl}}(n)]\hat{\mathbf{x}}(k_n, n) = \mathbf{q}. \tag{25}$$

The variable $\hat{\mathbf{x}}(k_n, n)$ is obtained by inverting equation (25). The spectral radial velocity, i.e., the sixth term of the vector $\hat{\mathbf{x}}(k_n, n)$, is thus equal to

$$\hat{v}_p(k_n, n) = \frac{|\mathbf{M}^{\mathrm{I}}_{1,6}|}{2\pi a|\mathbf{M}^{\mathrm{I}}|} F_p, \tag{26}$$

where

$$\mathbf{M}^{\mathrm{I}} = \mathbf{M}^{\mathrm{FI}} + \mathrm{j}k_n \mathbf{I}. \tag{27}$$

$\mathbf{M}^{\mathrm{I}}_{1,6}$ is the 9×9 matrix obtained from $\mathbf{M}^{\mathrm{I}}$ by suppressing line 1 and column 6.

Taking the inverse wavenumber transform of equation (26), the transfer mobility of the system for one particular circumferential mode n is

$$Y^n(z) = \frac{v_p(z, n)}{F_p} = \frac{1}{2\pi a} \int_{-\infty}^{+\infty} (|\mathbf{M}^{\mathrm{I}}_{1,6}|/|\mathbf{M}^{\mathrm{I}}|)\, \mathrm{e}^{-\mathrm{j}k_n z}\, \mathrm{d}k_n. \tag{28}$$

This integral is computed by utilizing a residue theorem, as performed by Fuller [3]; each of the residues being evaluated at the poles of the characteristic equation (9):

$$Y^n(z) = \frac{\mathrm{j}}{a} \sum_{s=1}^{\infty} \mathrm{Res}_n(s), \qquad \mathrm{Res}_n(s) = [|\mathbf{M}^{\mathrm{I}}_{1,6}|/(|\mathbf{M}^{\mathrm{I}}|)'] \, \mathrm{e}^{-\mathrm{j}k_n z}\Big|_{k_n = k_{ns}}, \tag{29, 30}$$

where the prime denotes the derivative with respect to k_n. Because of the singularities of the characteristic function near the zeros k_{ns}, numerically computing the derivative of the denominator would introduce an important error in the residue calculation. For this reason, a symbolic expression for the determinant of the matrix $\mathbf{M}^{\mathrm{I}}$, i.e., the characteristic equation, derived by Borgiotti *et al.* [10] is used:

$$|\mathbf{M}^{\mathrm{I}}| = \prod_{i=1}^{10} \mathrm{j}[k_n - \gamma(i, n)] + Z(k_n, n) \sum_{i=1}^{10} \left\{ \prod_{\substack{l=1 \\ l \neq i}}^{10} \mathrm{j}[k_n - \gamma(i, n)] \right\} e_6(i, n) f_1(i, n). \; \mathbf{2k} \tag{31}$$

In equation (31), $\gamma(i, n)$ are the ten roots of the system *in vacuo* (simple eigenvalue problem [9]), and $f_1(i, n)$ and $e_6(i, n)$ are, respectively, the first and sixth components of the normalized left and right eigenvectors associated with the eigenvalue $\gamma(i, n)$. Expression (31) is mostly polynomial and can be symbolically derived with respect to k_n.

The total mobility of the shell wall at one point $M(z, \varphi)$ is finally given by

$$Y(z, \varphi) = \sum_{n=0}^{\infty} \frac{\mathrm{j}\varepsilon_n \cos(n\varphi)}{a} \sum_{s=1}^{\infty} \mathrm{Res}_n(s). \tag{32}$$

where $\varepsilon_n = 1$ if $n = 0$ and $\varepsilon_n = 2$ if $n \neq 0$.

It is important to notice here that the two summations of equation (32) can be commuted. Therefore, it is not only possible to obtain the contribution of one particular circumferential mode n to the total response, but also the contribution of one particular wave type s, as introduced in the paper by Brévart and Fuller [13].

2.4. RESULTS

The shell system considered for numerical calculations has the same geometry and material properties as the mock-up described by Journeau [11], which is available for testing at the Commissariat à l'Energie Atomique (CEA), Cadarache, France. The

geometrical characteristics, material and fluid properties of the system are indicated in Table 1.

As in Journeau's work [11], approximate laws were used for the Bessel function of first and second kind, $J_n(x)$, $Y_n(x)$ and their derivatives, with large arguments n or x, based on formulae from the handbook by Abramowitz and Stegun [14].

2.4.1. *Roots of the characteristic equation*

To determine the roots of equation (9), we first consider the undamped system; i.e., a lossless shell filled with clear water. Similar to Fuller's work [2], an approximate location of the real roots is first determined by using a stepping procedure and testing the sign of the characteristic equation. The actual roots of the undamped system are found by using an algorithm that combines linear interpolation, inverse quadratic interpolation and the bisection method (IMSL subroutine DZBREN). Damping is then introduced in the shell material. The complex roots associated with this system are obtained from an algorithm using Müller's method with deflation, and the purely real roots of the undamped system as initial guesses (IMSL subroutine DZANLY). This procedure has also been recently used by other authors [5]. Then, damping is increasingly added to the fluid medium B, a small amount at a time, and the associated roots of equation (9) are used as initial guesses in a iterative manner until the desired amount of damping in medium B is achieved.

In Figure 3(a) are shown the dispersion curves obtained considering undamped waves of circumferential order $n = 1$ and non-dimensional frequencies $\Omega \leqslant 20$. For comparison, dispersion curves for the same shell *in vacuo* were also plotted, as well as the free acoustic wavenumber in the fluid medium. When the shell is *in vacuo* and vibrating in the $n = 1$ circumferential mode, only three waves can propagate undamped: a fast extensional wave, a torsional shear wave and a relatively slow flexural wave. When the shell is filled with water, 25 waves, denoted by a type order s which is related to the number of nodal lines along the radius, can propagate undamped; the $s = 1$ wave denotes the slowest wave in the system; i.e., the wave with the highest wavenumber. This wave approaches the *in vacuo* flexural solution at relatively low frequencies and, beyond the coincidence frequency (denoted "C" on Figure 3(a)) at which the wavelength of the *in vacuo* flexural wave is equal to the wavelength of the acoustic free wave in the fluid, the $s = 1$ wave tends asymptotically toward the fluid acoustic free wave. The higher order waves, $s = 2, 3, \ldots$, are characterized by a cut-on frequency and a "plateau" beahvior due to coincidences with the *in vacuo* extensional and torsional waves [2]; they eventually tend toward the fluid acoustic free wave at higher frequencies. Finally, it must be noted that only the wavenumber associated with the $s = 1$ wave is larger than the fluid acoustic wavenumber. Thus, the $s = 1$ wave does not radiate in the fluid field, whereas the higher order waves do.

TABLE 1

Geometrical characteristics, material and fluid properties

	Young's modulus (N/m^2)	Poisson ratio	Density (kg/m^3)	Damping ratio	Free wave speed (m/s)	Mid-fiber radius (m)	Shell thickness (m)
Steel shell	$19{\cdot}2 \times 10^{10}$	0·3	7800	0·001	5200	0·2	0·006
Water (medium A)	—	—	1000		1500	—	—
Bubbly water (medium B)	—	—	1000	0·02	1500	—	—

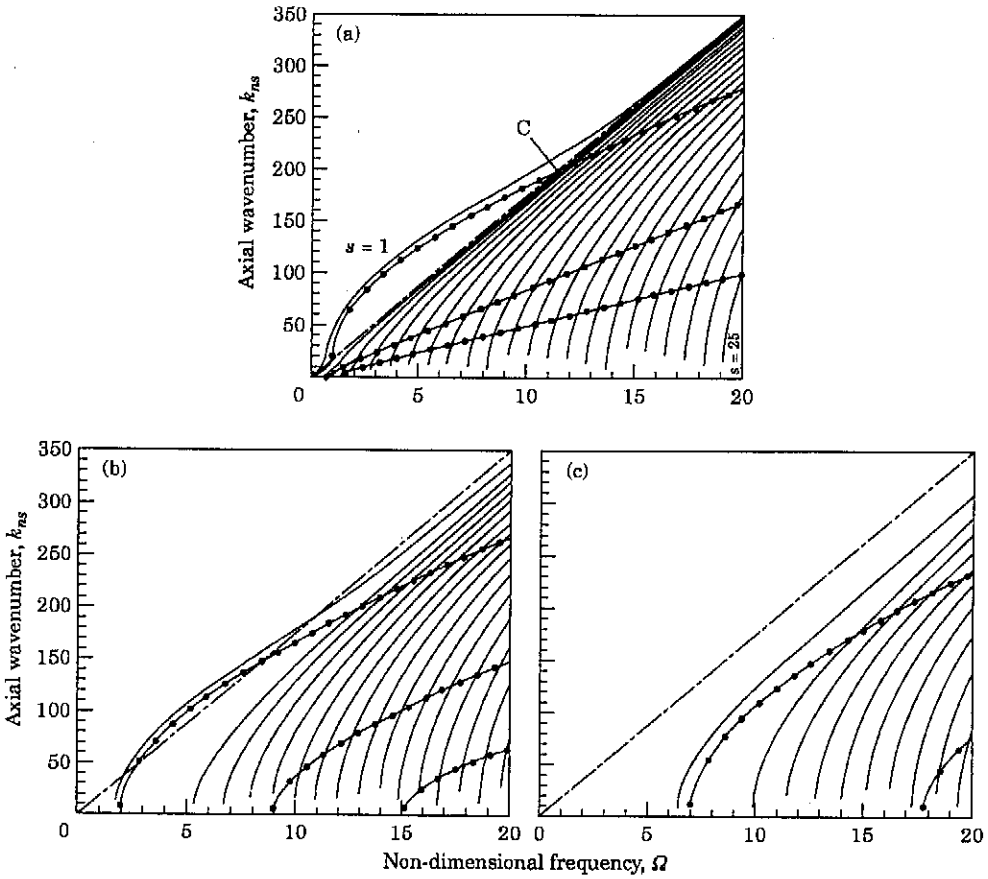

Figure 3. Dispersion curves (propagating waves): ——, Water-filled shell; —·—, shell *in vacuo*; – – –, free acoustic wavenumbers in water. (a) $n = 1$; (b) $n = 15$; (c) $n = 30$.

The dispersion curves associated with higher order circumferential modes appear similar to those for $n = 1$, but they reveal some significant differences. The dispersion curves obtained with $n = 15$ are shown in Figure 3(b). First, the *in vacuo* flexural wave has a non-zero cut on frequency, implying that the mode does not contribute to the response of the system *in vacuo* at low non-dimensional frequencies. At this point, it must be noted that the cut on frequency of the $s = 1$ wave, when the shell is filled with water, is lower than the cut on frequency of the *in vacuo* flexural wave. Finally, the coincidence of the

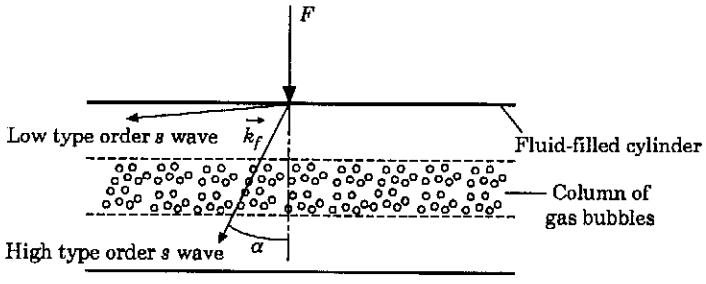

Figure 4. The s wave radiation angles.

in vacuo flexural wave with the acoustic free wave, as defined above, has been shifted to a lower frequency. Considering higher order modes, illustrated by the mode $n = 30$ in Figure 3(c), one can notice that the coincidence point between the *in vacuo* flexural wave and the acoustic free wave has disappeared. When the shell is filled with water, all the waves are supersonic and tend asymptotically toward the acoustic free wave.

The addition of 0·1% damping in the shell material has very little effect on the dispersion curves: all of the roots characterized above, which were purely real, now reveal a very small imaginary part associated with a slight attenuation of the wave amplitude as propagation occurs. The addition of 2% damping in the column of fluid medium B has a similar effect on the roots; i.e., increasing the imaginary part of the initially real roots. However, depending on the radius of the column and on the frequency of excitation, only certain waves s of circumferential order n are actually damped. To be more precise, fast waves,

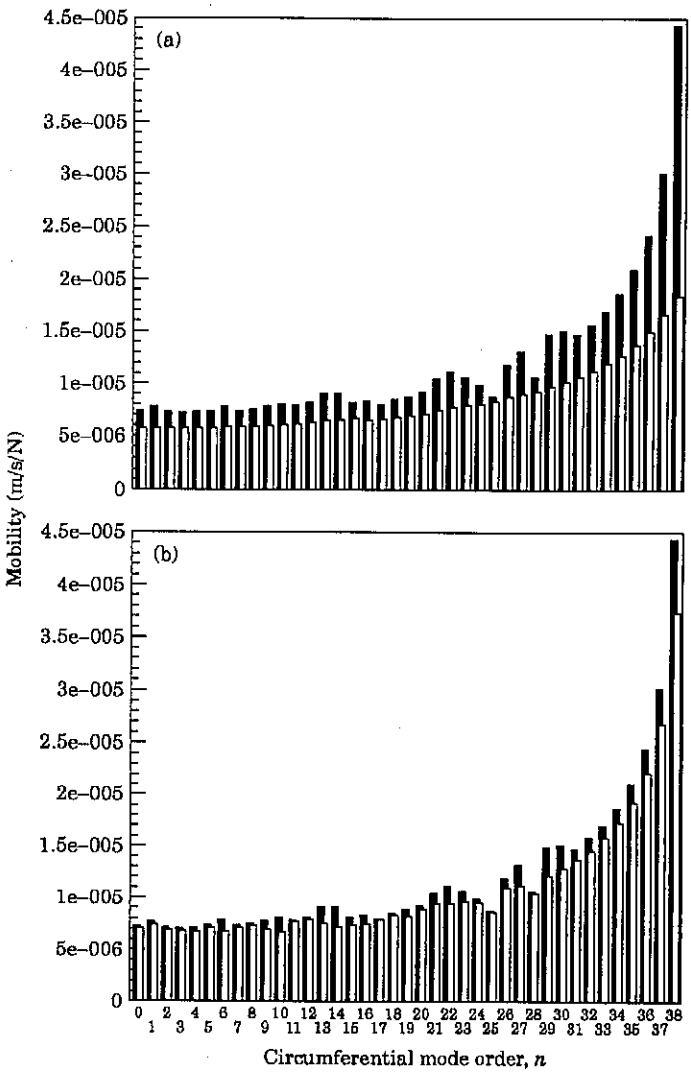

Figure 5. The mobility of the shell filled with water including a gas bubble column of radius a_c, for various circumferential mode orders $n,\Omega = 10$: black bars, $a_c = 0$; clear dotted bars, (a) $a_c = a - h/2$, (b) $a_c = 0{\cdot}95a$.

i.e., high s order waves, are affected by smaller gas columns than the slow waves, which are characterized by low type orders. This phenomenon can be explained in terms of acoustic radiation of the waves in the system. In Figure 4 are shown two wavenumber vectors associated with waves of low and high type order s. Note that the angle α of the vectors with a normal to the shell wall, also called the radiation angle [15], is defined as

$$\alpha = \arctan(k_{ns}/k^f_{ns}). \tag{33}$$

By examination of Figure 4, it becomes obvious that the pressure field associated with the high order s wave will be more affected by the presence of the damped column than the low order s wave, the wavenumber vector of which does not cross the gas column until very long axial distances.

2.4.2. *Forced response*

Considering the undamped system at the non-dimensional frequency $\Omega = 10$, there exists real roots of the characteristic equation (9), i.e., propagating waves, for circumferential mode orders n up to 38. In other words, if the system is excited by a point force, 39 circumferential modes will contribute to the response of the shell at one far-field point. In Figures 5(a) and (b) are shown the contributions of each of these modes one diameter away from the excitation, on the same azimuth as the point force, for various characteristics of the internal fluid. In Figure 5(a) is shown the modal decomposition of the response when there are either no gas bubbles in the fluid (medium A only) or gas bubbles uniformly distributed in the entire fluid (medium B only). In both cases, one can first notice that the shell response is dominated by waves of high circumferential order. The gas bubbles are seen to cause a fairly good attenuation on these modes, with a maximum 60% of attenuation on the mode $n = 38$. An average 20% of attenuation appears on modes with circumferential order below 28. Such a drop of magnitude in the shell mobility might eventually be detected by an appropriate array of sensors around the circumference. However, an efficient monitoring system is expected to

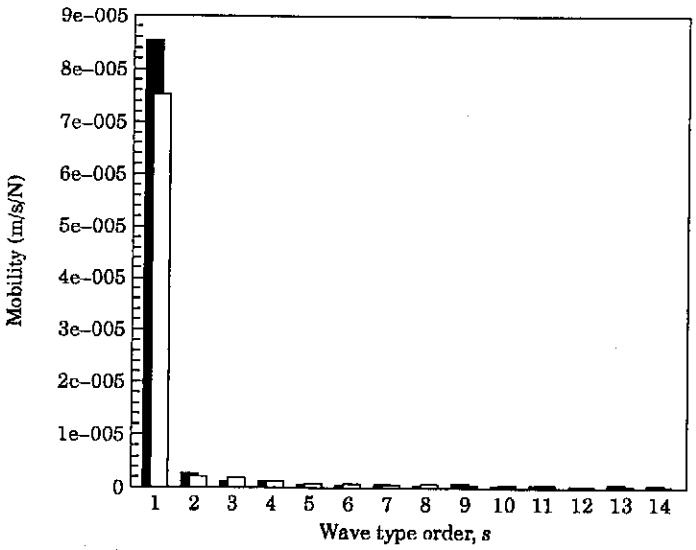

Figure 6. Wave type decomposition of the shell system point force mobility, $\Omega = 10$: black bars, $a_c = 0$; clear dotted bars, $a_c = 0{\cdot}95a$.

detect a gas leak as early as possible; i.e., before the gas bubbles are actually spread over the entire cylinder cross-section. In Figure 5(b) is shown the modal attenuation due to a smaller damped column in the fluid field, covering only 90% of the cylinder cross-section. The resulting attenuation of the various modes in the response one diameter from the source is very small, with a maximum 15% of attenuation on the circumferential mode $n = 38$. By reducing the volume of bubbly water by just 10%, the modal reductions were expected to be only slightly smaller than those in Figure 5(a). The explanation for this surprising result lies in the wave type decomposition of the response, shown in Figure 6. Among the 14 wave types contributing to the total resonse, only the $s = 1$ waves have a large amplitude. As discussed in the first section of this chapter, most of these waves have the particular characteristic of being subsonic in the fluid field; i.e., pressure near field at the shell wall. The $s = 1$ waves associated with high order

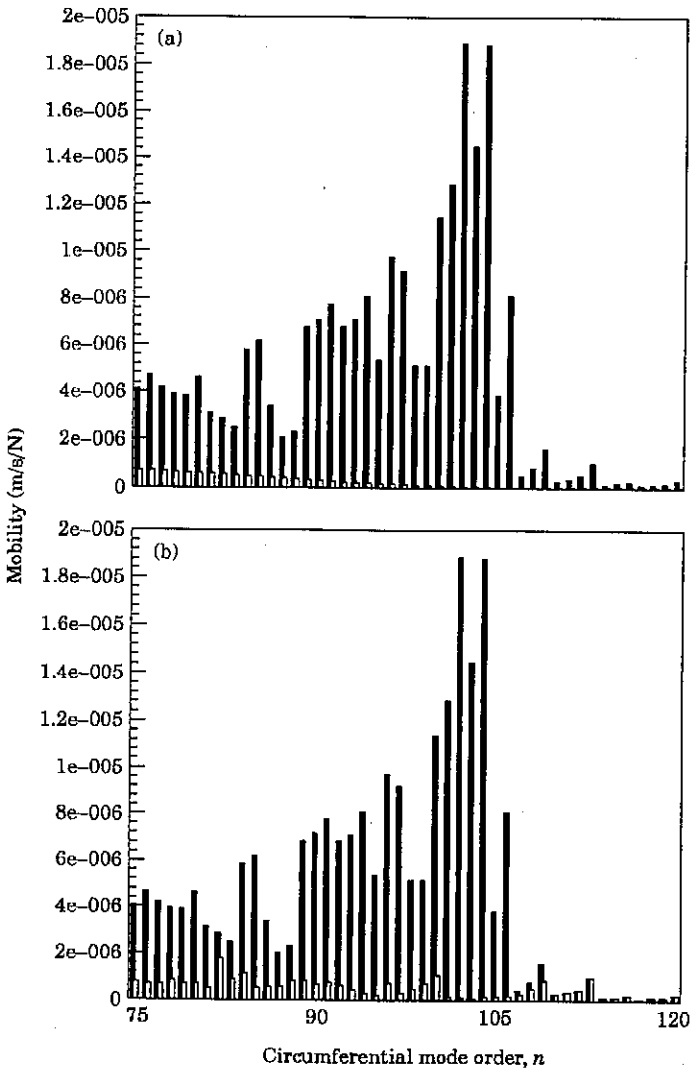

Figure 7. The mobility of the shell filled with water including a gas bubble column of radius a_c, for various circumferential mode orders $n,\Omega = 50$: black bars, $a_c = 0$; clear dotted bars, (a) $a_c = a - h/2$, (b) $a_c = 0{\cdot}65a$.

circumferential modes are supersonic waves but their phase speed approaches the acoustic free wave speed in the fluid; the radiation angle of these waves, defined by equation (33), is thus very large and the associated pressure field is not much affected by the gas column, as the results of Figure 5(b) indicate. Consequently, at the non-dimensional frequency $\Omega = 10$, the gas bubbles are quasi-uncoupled from the shell response unless they reach the near field of the shell wall. In other words, the presence of a small damped column can not be detected from the shell vibrations at this frequency.

At $\Omega = 50$, 167 circumferential modes are present in the total mobility of the shell wall. Among these, the contribution of the modes of circumferential order $n > 120$ is negligible. The contribution of the low order modes at this frequency is also relatively small. As the low order modes reveal little importance in the conclusions of this investigation, they are omitted. As a result, only the circumferential modes $n \in [75, 120]$ are considered at the frequency $\Omega = 50$. In Figure 7(a) is shown the modal decomposition of the response at $z = 2a$ and $\varphi = 0$, for two configurations of the fluid field; medium A only and medium B only. When no gas is present in the fluid, the mobility reaches a maximum for n between 100 and 104, then drops drastically as n is increased above 105. To explain this interesting behavior, we must consider the system *in vacuo*. When the cylindrical shell is *in vacuo*, only 105 circumferential modes can propagate undamped, due to the shift of the cut on frequencies of the waves discussed in section 2.4.1. As has been noticed, one realizes that the dominating waves in the fluid-filled system for one particular mode n are those approaching the *in vacuo* flexural wave of the same circumferential order (see dispersion curves in section 2.4.1). As there is no propagating wave of circumferential order $n > 104$ in the system *in vacuo* at $\Omega = 50$, the magnitude of the waves propagating when the shell is filled with water is relatively small. In Figure 7(a),

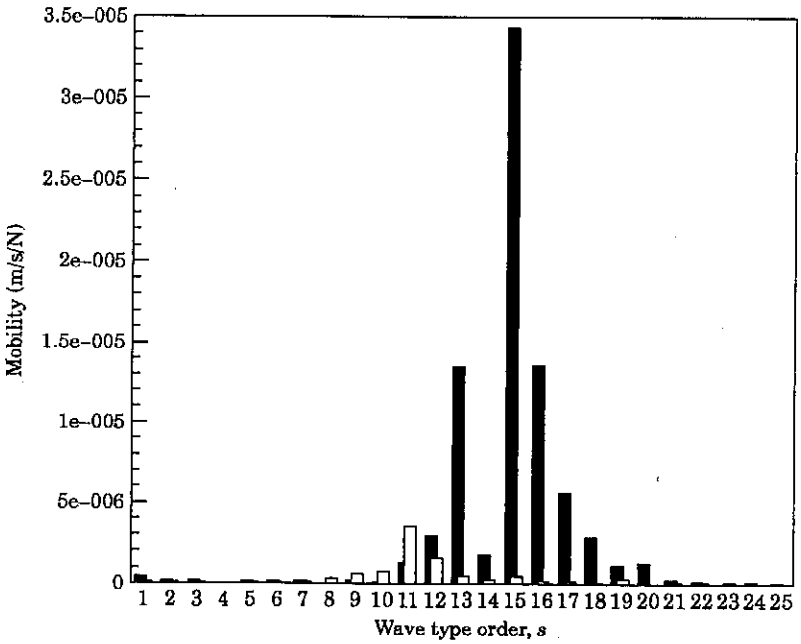

Figure 8. Wave type decomposition of the shell system point force mobility, $\Omega = 50$: black bars, $a_c = 0$; clear dotted bars, $a_c = 0{\cdot}65a$.

the attenuation caused by a uniform distribution of gas bubbles in the fluid field appears very large on all the circumferential modes. The attenuation is much larger than that obtained at $\Omega = 10$ because the wavelength of the dominating waves at $\Omega = 50$ is much smaller than one diameter, the distance from the source at which the response is evaluated. Considering a narrow column of bubbly water, covering 42% of the fluid cross section for example (Figure 7(b)), the shell velocity drop between two points only one diameter apart remains very important. These results are very different from those at $\Omega = 10$ because, as shown in Figure 8, the dominating waves in the system at this frequency have a type order s between 10 and 20, and all these waves radiate in the fluid field with a small radiation angle (see Fig. 4). When the size of the damped column is further decreased, the drop of the response at the axial position $z = 2a$ on the cylinder becomes non-uniform around the circumference because large order n modes are not attenuated. To illustrate this phenomenon, in Figures 9 and 10 are shown the modal and wave type decompostion of the shell response when the voume of bubbly water covers only 36% of the fluid cross-section ($a_c = 0{\cdot}6a$). It appears from Figure 10 that only the higher order type of wave are attenuated ($s > 15$), while the lower order types are not affected or even augmented (this last effect is due to the non-orthogonality of the s waves). The phase speed of the high order waves is large compared to the acoustic phase speed and the radiation angle of these waves is thus close to the normal at the wall; the main lobe of the radiated field inside the cylinder crosses the bubble column, whereas it does not for lower order types of wave (see Figure 4).

3. EXPERIMENTAL RESULTS

To assess the validity of the model described in section 2, various experiments were performed on a steam generator mock-up, the characteristics of which are very close to

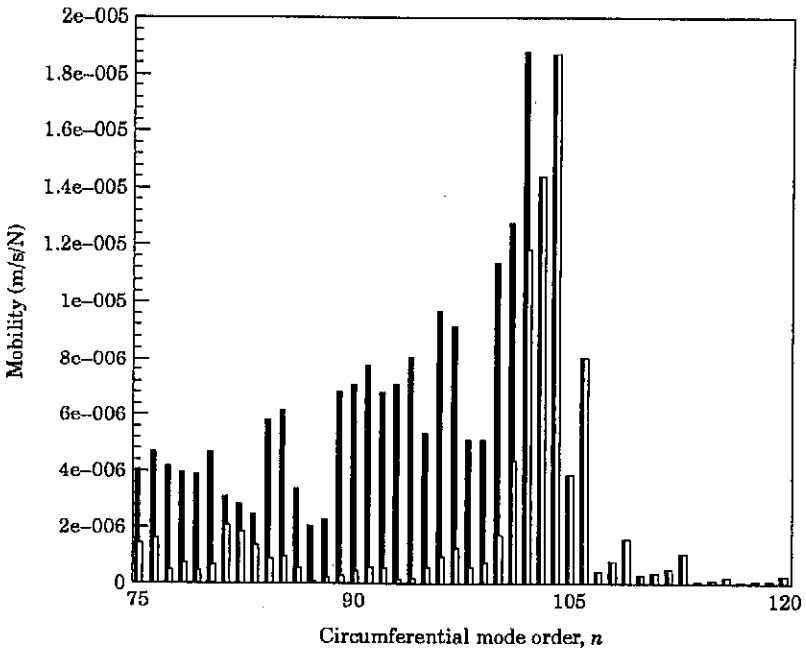

Figure 9. The mobility of the shell filled with water including a gas bubble column of radius a_c, for various circumferential mode orders $n, \Omega = 50$: black bars, $a_c = 0$; clear dotted bars, $a_c = 0{\cdot}60a$.

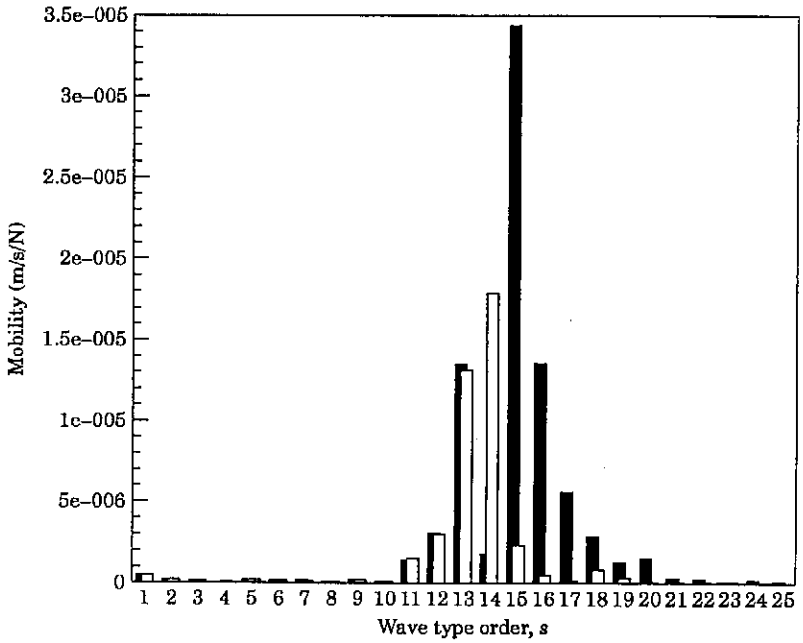

Figure 10. Wave type decomposition of the shell system point force mobility, $\Omega = 50$: black bars, $a_c = 0$; clear dotted bars, $a_c = 0{\cdot}60a$.

those used in the numerical calculations (see Table 1). A diagram of the experimental set-up is shown in Figure 11. The 18 m long cylinder is first filled with water that was stored in a tank for many days; the gas content of this water is thus very small. Two CEA constructed PZT transducers on 6 mm steel rods 3 m apart on the same azimuth are used as signal transmitter and receiver, respectively. An injection of gas is made possible 20 cm from one end of the cylinder through a 0·4 mm hole on a 15 mm pipe located at 180° from the transducers and about 5 cm from the shell wall. Note that this hole creates bubbles the size of which is within the assumptions made in section 2.2.

First, a white noise signal between 0 and 100 kHz is sent to transducer 1, generating a broadband "point force" on the cylinder. A power ratio (output power on transducer

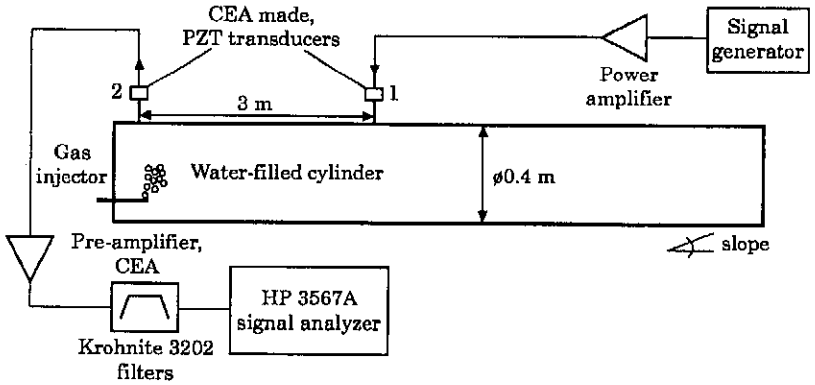

Figure 11. The experimental set-up.

2/input power on transducer 1) is evaluated, from 100 averages of the signals. A small amount of gas (8 bar pressure during 2 s) is then injected in the cylinder and the power ratio is re-evaluated. The results are shown in Figure 12. First, after the gas injection, a large increase of the output power appears between 0 and 30 kHz, because of the injector noise next to transducer 2. Between 30 kHz ($\Omega = 7{\cdot}3$) and 50 kHz ($\Omega = 12{\cdot}2$), the gas injection has no effect on the shell response. As expected from the analytical investigation, no attenuation of the shell response is obtained at $\Omega = 10$. Above 50 kHz, slight attenuations of the response appear, with a maximum 8 dB of attenuation around 100 kHz ($\Omega = 24{\cdot}4$).

The second set of experiments performed aim to determine the time evolution of the signal received in transducer 2 during an injection of gas when transducer 1 is periodically excited by a burst of sine waves at a particular frequency. First, a burst of 80 sine waves at 41 kHz ($\Omega = 10$) is sent to actuator 1 every tenth of a second. Before the gas injection, the individual r.m.s. signal received every 0·1 s by transducer 2 is steady, and is shown in Figure 13(a). In Figure 13(b) is shown the evolution of the major peak of the r.m.s. signal from burst to burst over 25 s. The gas injection occurs at 5 s. At this time, the main peak is seen to increase, because of the injector noise, to finally show a 10–15% attenuation by the end of the 25 s; by this time, most of the gas bubbles have reached the shell wall and are more likely to bring attenuation on the signal at this frequency. The evolution of a secondary peak of the r.m.s. signal is shown in Figure 13(c). This part of the r.m.s. signal experiences a fast decrease followed by an increase to finally reach a 70% attenuation after 25 s. It is believed that this part

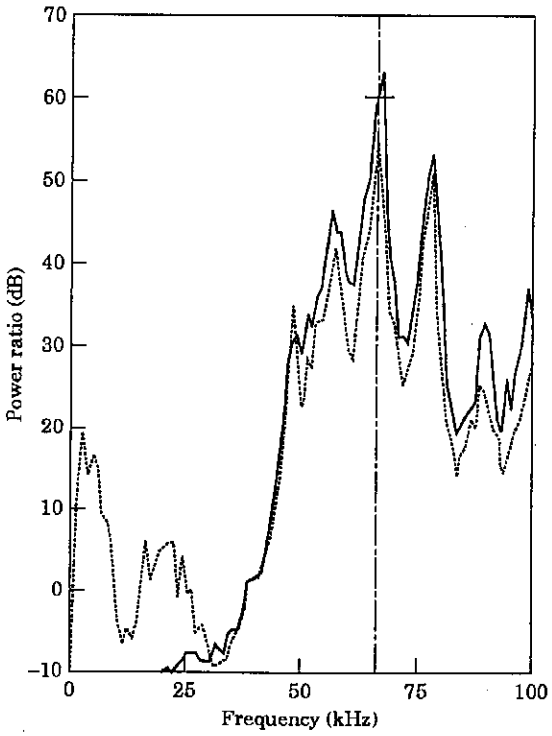

Figure 12. The power ratio (output power at transducer 2 divided by input power at transducer 1), white noise excitation on mock-up. ——, Before gas injection;.....,after gas injection (8 bar pressure, 2s).

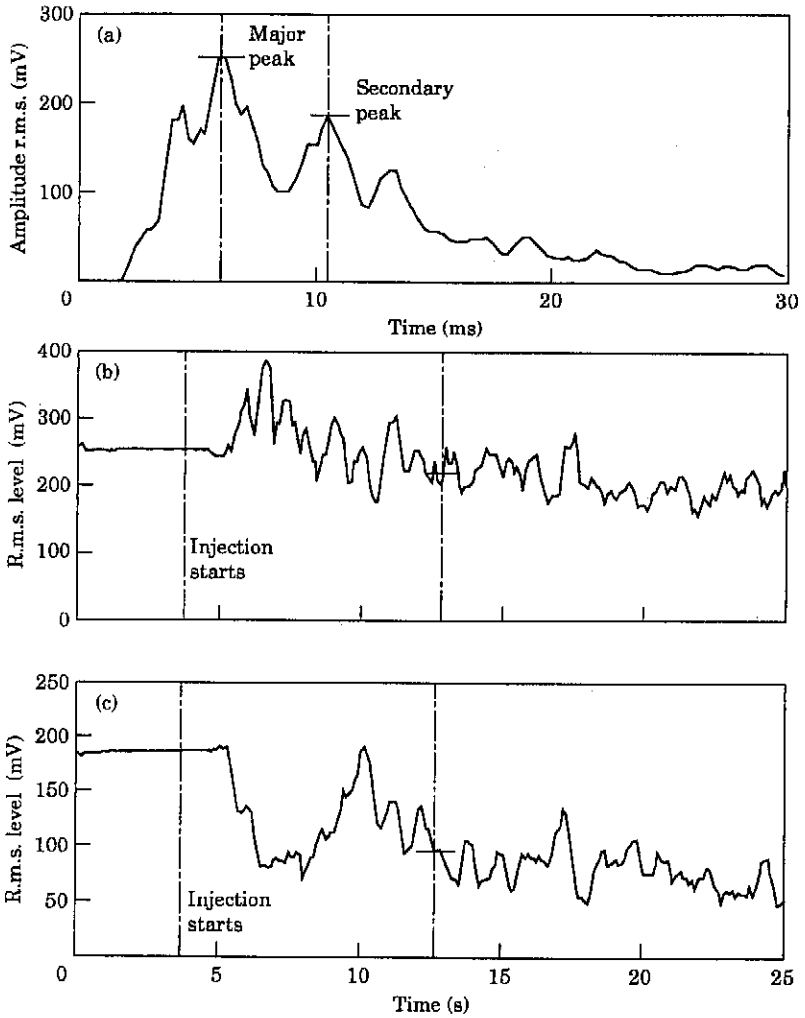

Figure 13. Burst excitation, 80 sine waves at 41 kHz ($\Omega = 10$), 0·1 s recurrence. (a) The r.m.s. signal received after one burst before injection; (b) the major peak of the r.m.s. signal as a function of time; (c) the secondary peak of the r.m.s. signal as a function of time.

of the r.m.s. signal is mainly due to the $s = 1$ waves of high circumferential order, which are more attenuated by the gas bubbles, especially if they reach the shell wall, as seen in section 2.4.2.

In Figure 14, a burst of 400 sine waves at 206 kHz ($\Omega = 50$) is now sent to actuator 1 every tenth of a second. After the gas injection at 5 s, the major peak of the r.m.s. signal before injection in Figure 14(a) is drastically attenuated by almost 50% within 2 or 3 seconds (see Figure 14(b)). A late secondary peak of the r.m.s. signal in Figure 14(a) is also heavily decreased (see Figure 14(c)). In fact, the whole signal in Figure 14(a) experiences a large attenuation within seconds of gas injections. The attenuation caused by the gas injection on the signal at the non-dimensional frequency $\Omega = 50$ is thus global, as expected from the numerical calcualtions. This result reveals the potential of the active acoustic gas leak detection method [1] at very high frequencies.

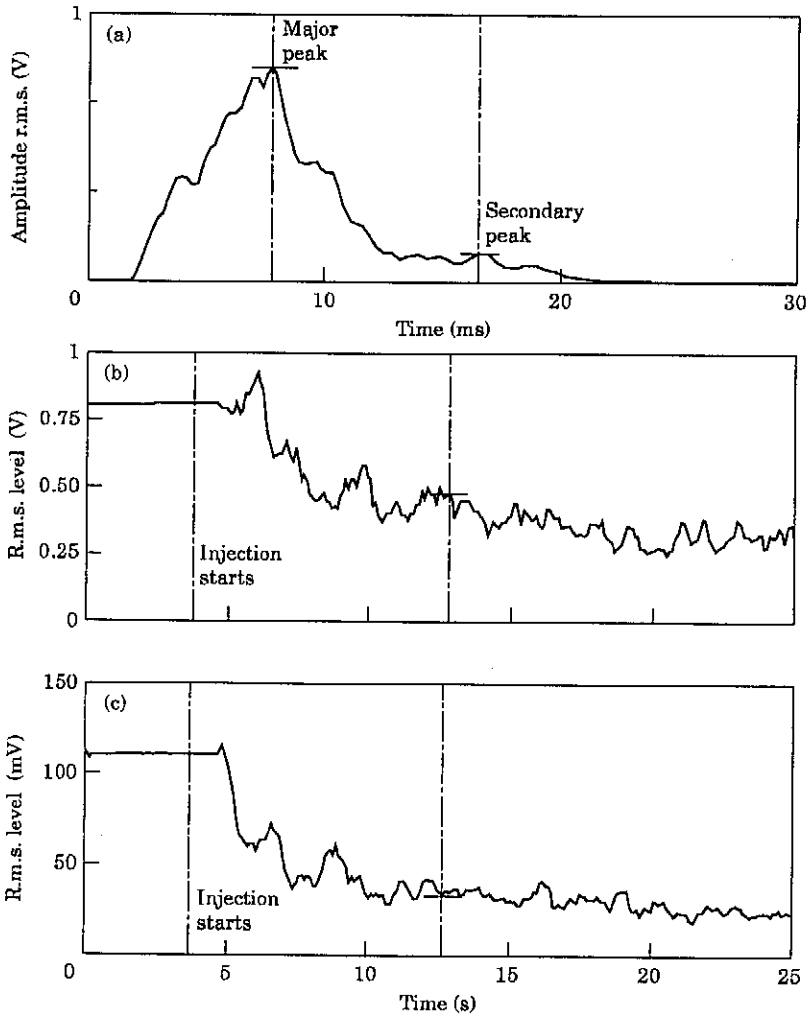

Figure 14. Burst excitation, 400 sine waves at 206kHz ($\Omega = 50$), 0·1s recurrence. (a) The r.m.s. signal received after one burst before injection; (b) the major peak of the r.m.s. signal as a function of time; (c) the secondary peak of the r.m.s. signal as a function of time.

4. CONCLUSIONS

The high frequency harmonic response to a point force of a cylindrical elastic shell filled with a fluid including a damped column representing gas bubbles has been analytically investigated. The results at various frequencies have been analyzed and explained in terms of wave contributions for various configurations of the gas column. In particular, it has been noticed that the dominant waves of a particular circumferential order n in the system are those, the characteristics of which approach the *in vacuo* flexural solution of the same circumferential order. For example, at $\Omega = 10$, the response of the system is dominated by $s = 1$ waves of circumferential order varying from 0 to 38. These waves are either subsonic or radiate in the fluid field with a very large radiation angle. Consequently, it is difficult to detect the presence of gas bubbles at this frequency unless the bubbles are near the shell wall. At $\Omega = 50$, the system response is dominated by higher order type of waves

($s = 14, 15, \ldots$) which radiate in the fluid field with small angles. As a result, relatively small columns of gas bubbles can externally be detected by the attenuation they bring to the shell response.

Various experimental investigations have revealed the same trend. First, a broadband approach has shown that a small leak of gas bubbles in the water filled cylinder considered has little attenuating effect on the transmitted signal at frequencies below $\Omega = 12$; however, the attenuation was found to increase at higher frequencies. Two series of experiments on signal transmission through the shell system at discrete frequencies have also been performed. At $\Omega = 50$, 8–14 dB attenuation of the entire transmitted signal was obtained within 2 or 3 seconds after the gas injection, whereas only partial attenuation of the transmitted signal appeared at $\Omega = 10$; at this frequency, only a few waves, corresponding to the highest circumferential mode orders, were affected by some gas bubbles at or near the shell wall.

Through the theoretical and experimental results obtained for this particular shell system, the importance of the frequency of excitation on the performance of the active acoustic gas leak detection [1] method has been demonstrated.

ACKNOWLEDGMENTS

This work was partially supported by Electricité de France and Framatome through co-operative actions 4705 and 4477. Thanks are due to Raynald Démarais for his assistance in the experimental work.

REFERENCES

1. P. GARNAUD and R. DÉMARAIS 1990 *French Patent* 90 00934.
2. C. R. FULLER and F. J. FAHY 1982 *Journal of Sound and Vibration* **81**, 501–518. Characteristic of wave propagation and energy distribution in cylindrical elastic shells filled with fluid.
3. C. R. FULLER 1983 *Journal of Sound and Vibration* **87**, 409–427. The input mobility of an infinite circular cylindrical elastic shell filled with fluid.
4. C. R. FULLER 1984 *Journal of Sound and Vibration* **96**, 101–110. Monopole excitation of vibrations in an infinite cylindrical elastic shell filled with fluid.
5. G. F. LEYRAT 1990 *Ph.D. Dissertation, Florida Atlantic University*. Effects of an internal flow on the vibration of thin cylindrical shells.
6. B. J. BRÉVART and C. R. FULLER 1993 *Journal of Sound and Vibration* **167**, 149–163. Effect of an internal flow on the distribution of vibrational energy in an infinite fluid-filled thin cylindrical elastic shell.
7. L. FENG 1996 *Journal of Sound and Vibration*, **189**(4), 511–524. Experimental studies on the acoustic properties of a finite elastic pipe filled with water/air.
8. L. FENG 1993 *Proceedings of Internoise* 93, *Leuven, Belguim*, II, 1219–1222. Influences of absorptive layer on vibration and noise levels of water filled elastic pipes.
9. G. V. BORGIOTTI and E. M. ROSEN 1992 *Journal of the Acoustical Society of America* **92**(2), 911–925. The state vector approach to the wave and power flow analysis of the forced vibrations of a cylindrical shell, part I: infinite cylinders in vacuum.
10. G. V. BORGIOTTI and E. M. ROSEN 1994 *Journal of the Acoustical Society of America*, **95**(1), 244–255. Power flow analysis of surface waves on a cylindrical elastic shell in an acoustic fluid.
11. C. JOURNEAU 1995 *Journal of the Acoustical Society of America* **97**(3), 1670–1677. High frequency vibration of liquid filled thick elastic cylinders: a simplified modal approach.
12. E. SILBERMAN 1957 *Journal of the Acoustical Society of America* **29**, 925–933. Sound velocity and attenuation in bubbly mixtures measured in standing wave tubes.
13. B. J. BRÉVART and C. R. FULLER 1994 *Journal of Sound and Vibration* **177**, 411–422. Radial impulsive excitation of infinite fluid-filled elastic cylindrical shells.

14. M. ABRAMOWITZ and I. A. STEGUN 1965 *Handbook of Mathematical Functions*. New York: Dover.
15. M. C. JUNGER and D. FEIT 1986 *Sound, Structures and their Interaction*. Cambridge, MA: MIT Press.

APPENDIX A: ELEMENTS OF MATRICES

The matrix $\mathbf{M}(n)$ is defined as

$$\mathbf{M}(n) = \mathbf{A}(n) - \mathbf{B}(n)\mathbf{D}^{-1}\mathbf{C}(n),$$

where

$$\mathbf{A}(n) = \begin{bmatrix}
0 & 0 & 0 & 0 & 0 & j\omega\rho_m h & 0 & 0 & 0 & 0 \\
0 & 0 & 0 & 0 & 0 & 0 & j\omega\rho_m h & 0 & 0 & 0 \\
0 & 0 & 0 & 0 & 0 & 0 & 0 & j\omega\rho_m h & 0 & 0 \\
1 & 0 & 0 & 0 & 0 & 0 & 0 & 0 & j\omega\rho_m h & 0 \\
0 & 0 & 0 & 0 & 0 & 0 & 0 & 0 & 0 & j\omega\rho_m h \\
\frac{j\omega 2(1+\nu)}{Eh} & 0 & 0 & 0 & 0 & 0 & 0 & 0 & -1 & 0 \\
0 & 0 & 0 & 0 & 0 & 0 & 0 & j\frac{n}{a} & 0 & 0 \\
0 & 0 & \frac{j\omega(1-\nu^2)}{Eh} & 0 & 0 & -\frac{\nu}{a} & -j\frac{n\nu}{a} & 0 & 0 & 0 \\
0 & 0 & 0 & \frac{j\omega(1-\nu^2)}{EJ} & 0 & 0 & 0 & 0 & 0 & -j\frac{n\nu}{a} \\
0 & 0 & 0 & 0 & 0 & 0 & 0 & 0 & -j\frac{n}{a} & 0
\end{bmatrix},$$

$$\mathbf{B}(n) = \begin{bmatrix}
-\frac{jn}{a} & \frac{1}{a} & 0 & 0 & 0 \\
-\frac{1}{a} & -\frac{jn}{a} & 0 & 0 & 0 \\
0 & 0 & -\frac{jn}{a} & 0 & 0 \\
0 & 0 & 0 & -\frac{jn}{a} & 0 \\
1 & 0 & 0 & 0 & -\frac{jn}{a} \\
0 & 0 & 0 & 0 & 0 \\
0 & 0 & \frac{j\omega 2(1+\nu)}{Eh} & 0 & 0 \\
0 & 0 & 0 & 0 & 0 \\
0 & 0 & 0 & 0 & 0 \\
0 & 0 & 0 & \frac{j\omega 2(1+\nu)}{EJ} & 0
\end{bmatrix},$$

$$\mathbf{C}(n) = \begin{bmatrix} 0 & -1 & 0 & 0 & 0 & 0 & 0 & 0 & 0 & 0 \\ 0 & 0 & -\nu & 0 & 0 & -\dfrac{Eh}{j\omega a} & -\dfrac{nEh}{\omega a} & 0 & 0 & 0 \\ 0 & 0 & 0 & 0 & 0 & -\dfrac{nEh}{2\omega a(1+\nu)} & \dfrac{Eh}{j2\omega a(1+\nu)} & 0 & 0 & -\dfrac{Eh}{j2\omega a(1+\nu)} \\ 0 & 0 & 0 & 1 & 0 & 0 & 0 & 0 & 0 & \dfrac{nEj}{\nu a\omega} \\ 0 & 0 & 0 & 0 & 0 & 0 & 0 & 0 & 0 & 0 \end{bmatrix},$$

$$\mathbf{D}(n) = \begin{bmatrix} 0 & 0 & 1 & 1/a & 0 \\ 0 & 1 & 0 & 0 & 0 \\ 1 & 0 & 0 & 0 & 0 \\ 0 & 0 & 0 & 0 & -1/\nu \\ 0 & 0 & J/ah & 1 & 0 \end{bmatrix}.$$

APPENDIX B: LIST OF SYMBOLS

a	shell mid-fiber radius	$M_{z\varphi}$	twisting moment per unit circumferential length in the ρ–φ plane
a_c	radius of medium A–medium B interface	n	circumferential mode order
c_f	free wave speed in lossless medium A	N_z	normal force resultant per unit circumferential length
c_f^d	free wave speed in medium B	$p(z, n)$	acoustic pressure at the shell wall
c_L	shell extensional phase speed	$P_f^d(z, r, \varphi)$	acoustic pressure in fluid medium B
$\mathbf{e}^s(n)$	modal vector	$P^f(z, r, \varphi)$	acoustic pressure in fluid medium A
E	Young's modulus	$P_{ns}^d, P_{ns}^f, Q_{ns}^f$	pressure amplitudes
h	shell thickness	s	branch number, wave type order
$\mathbf{I}$	identity matrix	$\mathrm{Res}_s(n)$	residue associated with k_{ns}
j	$=\sqrt{-1}$	$T_{z\rho}, T_{z\varphi}$	shear force resultants per unit circumferential length
J	$=h^3/12$, geometric moment of inertia of the shell with respect to the mid-fiber per unit length	v_ρ, v_φ, v_z	mid-fiber velocities
J_n	Bessel function of first kind of order n	$x_a^f, x_A^d, x_B^f, x_B^d$	non-dimensional radial wavenumbers
k_n	axial wavenumber	$Z(k_{ns}, n)$	acoustic impedance at the shell wall
k_{ns}	axial wavenumber of the branch s	Y^n	modal mobility
k_{rns}^d	radial wavenumber of the branch s in medium B	Y_n	Bessel function of second kind of order n
k_{rns}^f	radial wavenumber of the branch s in medium A	$Y(z, \varphi)$	total mobility
M_z	bending moment per unit circumferential length in the ρ–z plane		

β	attenuation constant of fluid medium B	ρ_f	specific mass of fluid medium A
ε_n	$=1, n=0$ or $=2, n\neq 0$	ω	circular frequency
$\gamma(i,n)$	eigenvalues of *in vacuo* system	Ω	$=\omega a/c_L$, non-dimensional frequency
ν	Poisson ratio	Ω_z, Ω_φ	angular velocities in the ρz and $\rho-\varphi$ planes
ρ, z, φ	cylindrical co-ordinates		
ρ_d	specific mass of fluid medium B	$(\hat{})$	wavenumber transform